# Stochastic Modeling of Flexible Rotors

**Edson H. Koroishi**
koroishi@mecanica.ufu.br

**Aldemir Ap. Cavalini, Jr.**
aacjunior@mecanica.ufu.br

**Antônio M. G. de Lima**
amglima@mecanica.ufu.br

**Valder Steffen, Jr.**
vsteffen@mecanica.ufu.br
Federal University of Uberlândia
School of Mechanical Engineering
38408-100 Uberlandia, MG, Brazil

*Flexible rotors are characterized by inherent uncertainties affecting the parameters that influence the dynamic responses of the system. In this context, the handling of variability in rotor dynamics is a natural and necessary extension of the modeling capability of the existing techniques of deterministic analysis. Among the various methods used to model uncertainties, the stochastic finite element method has received major attention, as it is well adapted for applications involving complex engineering systems of industrial interest. In the present contribution, the stochastic finite element method applied to a flexible rotor system, with random parameters modeled as random fields is presented. The uncertainties are modeled as homogeneous Gaussian stochastic fields and are discretized according to the spectral method by using Karhunen-Loève expansions. The modeling procedure is confined to the frequency and time domain analyses, in which the envelopes of frequency response functions, the Campbell's diagram and the orbits of the stochastic flexible rotor system are generated. Also, Monte Carlo simulation method combined with the Latin Hypercube sampling is used as stochastic solver. After the presentation of the underlying theoretical formulations, numerical applications of moderate complexity are presented and discussed aiming at demonstrating the main features of the stochastic modeling procedure of flexible rotor systems.*
***Keywords:*** *uncertainty quantification, rotor dynamics, stochastic finite elements*

## Introduction

In the development of many types of engineering products, an increasing demand for durability, reliability, safety, comfort, low cost manufacturing and fast solutions time is observed. As a result, during the design phase or during the analysis of an existing system, there is a compromise between the operational conditions and the vibration and noise levels, which are important aspects to be considered in up-to-date engineering.

In the context of new rotor dynamics design, in the last decades, much effort has been devoted to the development of deterministic models capable of accounting for the typical variations of construction features and material properties of flexible rotors. The understanding of the dynamic behavior of such systems has been investigated under several aspects. Comprehensive studies on this subject have been reported in the monographs by Lallane and Ferraris (1998) and Vance et al. (2010).

A natural extension of the deterministic modeling procedure is to account for the uncertainties in physical and/or geometrical parameters aiming at evaluating the degree of influence of variability on the performance predictions. Such uncertainty analysis becomes especially interesting for improving model reliability for various purposes, such as, system identification (Assis et al., 2003), balancing (Saldarriaga et al., 2010), crack and fatigue damage analyses (Morais et al., 2008), active vibration control and optimal design (Simões et al., 2007; Lei et al., 2008; Koroishi et al., 2011). As an example, Ritto et al. (2011) have considered uncertain parameters in order to propose a new performance optimization methodology for flexible rotors. Rémond et al. (2011) have studied the dynamics of a flexible rotor system assessing uncertain parameters by using the so-called Polynomial Chaos Expansion (PCE) technique (Ghanem and Spanos, 1991). The results obtained have been compared with those from the Monte Carlo simulation (MC) to assess response variability.

It is important to mention that most of those studies claim that one of the main limitations in taking uncertainty propagation into account in structural dynamics is the high computational cost that results from the necessity of computing a large number of response samples to achieve the necessary statistical significance. Moreover, few works, such as the one in reference (Ritto et al., 2011), have addressed the influence of uncertainties on the response variability of flexible rotors, in which *ad-hoc* procedures must be used to cope with the variations in the physical and/or geometrical parameters.

Starting from the previous contributions regarding the deterministic modeling of flexible rotors, the present paper intends to propose a stochastic finite element modeling of a flexible rotor, for which a parameterization approach has been suggested in such a way to enable the introduction of parametric variations in a straightforward manner. Also, a model condensation strategy specially adapted to flexible rotor systems, in which the dynamic response of the rotor is projected on a truncated modal basis of the non-gyroscopic associated conservative system, has been used. Numerical simulations are carried-out to appraise the response variability in terms of the envelopes of the frequency response functions (FRFs), the Campbell diagram and the orbits for the different uncertainty scenarios.

## Nomenclature

| | |
|---|---|
| $\boldsymbol{M}$ | = *mass matrix, kg* |
| $\boldsymbol{K}$ | = *stifness matrix, N/m* |
| $\boldsymbol{C}$ | = *viscous damping matrix, N.s/m* |
| $\boldsymbol{G}$ | = *gyroscopic matrix, kg/s* |
| $\overline{\boldsymbol{M}}$ , $\overline{\boldsymbol{K}}$ , $\overline{\boldsymbol{C}}$ , $\overline{\boldsymbol{G}}$ | = *parameterized matrices* |
| $\boldsymbol{q}(t)$ | = *vector of the generalized displacements, m* |
| $\boldsymbol{F}(t)$ | = *vector of the generalized loads, N* |
| $\boldsymbol{H}(\omega,\Omega)$ | = *frequency response function matrix* |
| $\boldsymbol{N}(y)$ | = *matrix containing the shape functions* |
| $\boldsymbol{B}(y)$ | = *matrix formed by the differential operators* |
| $\boldsymbol{E}$ | = *matrix of the isotropic material properties, Pa* |
| $\boldsymbol{T}$ | = *nominal reduction basis* |
| $H(y,\theta)$ | = *random field* |
| $C(y_1,y_2)$ | = *covariance function* |
| $f_r(y)$ , $\lambda_r$ | = *eigenfunction and eigenvalue of the covariance* |
| $E$ | = *Young's modulus, N/m* |
| $N$ | = *number of global degrees of freedom (DOFs)* |

**Paper received 27 April 2012. Paper accepted 24 August 2012.**

**Greek Symbols**

$\Omega$ = *rotor speed, rad/s*
$\omega$ = *excitation frequency, rad/s*
$\alpha$ = *proportional coefficient of mass matrix*
$\beta$ = *proportional coefficient of stiffness matrix*
$\Omega_{KL}$ = *geometric domain, m*
$\theta$ = *random process*
$\rho$ = *mass density, kg/m³*
$\xi_r(\theta)$ = *random variable*

**Subscripts**

*B* = *bearing*
*D* = *disk*
*S* = *shaft*
*P* = *proportional damping*
*e* = *finite element*

## Deterministic Modeling of a Flexible Rotor

In this section, the formulation of a flexible rotor finite element composed of a shaft, rigid discs and bearings is summarized based on the original developments made by Lallane and Ferrraris (1998). Figure 1 depicts the beam element used to model the shaft composed of two nodes, and four degrees of freedom (DOFs) per node, representing the nodal displacements along the *x* and *z* directions (denoted by $u$ and $w$, respectively) and the cross-section rotations about axes *x* and *z* axes (denoted by $\theta = \partial w/\partial y$ and $\psi = \partial u/\partial y$, respectively).

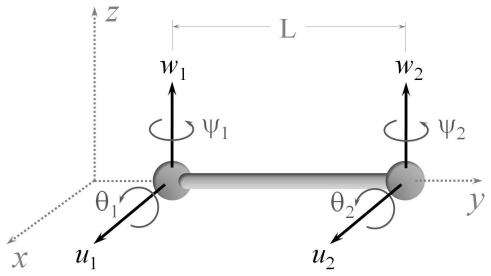


**Figure 1. Illustration of the shaft finite element.**

In the development of the theory, the following assumptions are adopted: (*i*) the material involved is homogeneous and isotropic and present linear mechanical behavior; (*ii*) the beam element is modeled according to Euler-Bernoulli's theory (transverse shear is neglected); (*iii*) the effects of inertial rotations are taken into account.

The discretization of the displacement fields within the element is made by using cubic interpolation functions for the translational displacements $u$ and $w$, according to the general relation $\boldsymbol{u}(y,t) = \boldsymbol{N}(y)\,\boldsymbol{u}_{(e)}(t)$, where $\boldsymbol{N}(y)$ is the matrix formed by the shape interpolation functions, and $\boldsymbol{u}_{(e)}(t) = [u_i\ w_i\ \theta_i\ \psi_i]^T$ with $i = 1 \text{ to } 2$ represents the vector containing the mechanical nodal variables as a function of time. The strain-displacement relations $\boldsymbol{\varepsilon}(y,t) = \boldsymbol{B}(y)\boldsymbol{u}_{(e)}(t)$ are used and the resulting strains for the beam element are generated.

Following standard analytical developments of variational principles, the strain and kinetic energies of the beam finite element can be formulated and the elementary mass, gyroscopic and stiffness matrices are obtained, respectively, as follows:

$$\boldsymbol{M}_S^{(e)} = \int_{y=0}^{L} \boldsymbol{N}_{mi}^T(y)\boldsymbol{N}_{mi}(y)dy \tag{1.a}$$

$$\boldsymbol{G}_S^{(e)} = \int_{y=0}^{L} \boldsymbol{N}_g^T(y)\boldsymbol{N}_g(y)dy \tag{1.b}$$

$$\boldsymbol{K}_S^{(e)} = \int_{y=0}^{L} \boldsymbol{B}^T(y)\boldsymbol{E}\,\boldsymbol{B}(y)dy \tag{1.c}$$

where $\boldsymbol{M}_S^{(e)} \in R^{N_e \times N_e}$ is the elementary mass matrix formed by the contributions of the mass and the inertia of the shaft element, $\boldsymbol{G}_S^{(e)} \in R^{N_e \times N_e}$ designates the gyroscopic matrix, $\boldsymbol{K}_S^{(e)} \in R^{N_e \times N_e}$ represents the stiffness matrix, and $\boldsymbol{E}$ is the isotropic matrix containing the elastic material properties. Matrix $\boldsymbol{B}(y)$ is formed by differential operators appearing in the strain-displacement relations, and $\boldsymbol{N}_{mi}^T$ and $\boldsymbol{N}_g^T$ represent, respectively, the mass and inertia contributions on the matrix formed by the shape interpolation functions. $N_e = 8$ is the number of elementary DOFs.

At this point, the contribution of a rigid disc on the system can be introduced by formulating its kinetic energy associated with the node of attachment *nd* in the elementary coordinate system, where $\boldsymbol{M}_D^{(e)} \in R^{N_e \times N_e}$ represents the elementary mass matrix of the rigid disc, and $\boldsymbol{G}_D^{(e)} \in R^{N_e \times N_e}$ designates its gyroscopic matrix. Also, the inclusion of the stiffness and damping effects of the bearings can be easily done by using the concept of dyadic structural modifications (Maia and Montalvão e Silva, 1997), in which the force vector is first written as $\boldsymbol{f}_B(t) = \boldsymbol{K}_B\boldsymbol{q}(t) + \boldsymbol{C}_B\dot{\boldsymbol{q}}(t)$, where $\boldsymbol{K}_B = \boldsymbol{I}_p^T\boldsymbol{K}_B^{nd}\boldsymbol{I}_p$ and $\boldsymbol{C}_B = \boldsymbol{I}_p^T\boldsymbol{C}_B^{nd}\boldsymbol{I}_p$, and $\boldsymbol{I}_p$ designates the *p*-th column of the identity matrix of order *N*, according to the node of attachment.

From the elementary finite element matrices computed for each element, and assuming that the flexible rotor presents inherent proportional damping, the global system of equations of motion for the system containing $N$ DOFs are constructed accounting for node connectivity, using standard FE assembling procedures:

$$\boldsymbol{M}\,\ddot{\boldsymbol{q}}(t) + (\boldsymbol{C} + \Omega\boldsymbol{G})\dot{\boldsymbol{q}}(t) + \boldsymbol{K}\,\boldsymbol{q}(t) = \boldsymbol{F}(t) \tag{2}$$

where $\boldsymbol{M} = (\boldsymbol{M}_S + \boldsymbol{M}_D) \in R^{N \times N}$ and $\boldsymbol{K} = (\boldsymbol{K}_S + \boldsymbol{K}_B) \in R^{N \times N}$ represent, respectively, the mass and stiffness matrices, $\boldsymbol{C} = (\boldsymbol{C}_B + \boldsymbol{C}_p) \in R^{N \times N}$ is the damping matrix formed by the contributions of the viscous damping matrix, $\boldsymbol{C}_B$, and the inherent proportional damping matrix, $\boldsymbol{C}_p = \alpha\boldsymbol{M} + \beta\boldsymbol{K}$, and $\boldsymbol{G} = (\boldsymbol{G}_D + \boldsymbol{G}_S) \in R^{N \times N}$ designates the gyroscopic matrix formed by the gyroscopic contributions of the rigid discs and the shaft. $\boldsymbol{q}(t) \in R^N$ and $\boldsymbol{F}(t) \in R^N$ are, respectively, the vectors of the amplitudes of the harmonic generalized displacements and external loads, $\Omega$ is the angular speed of the shaft, and $\alpha$ and $\beta$ represent, respectively, the proportional coefficients of mass and stiffness.

The interest herein is also focused on frequency domain responses. In this case, Eq. (2) can be directly used for calculating

the steady-state harmonic responses of the rotor in the frequency domain, by assuming $\boldsymbol{F}(t)=\boldsymbol{F}(\omega)e^{i\omega t}$ and $\boldsymbol{q}(t)=\boldsymbol{Q}(\omega,\Omega)e^{i\omega t}$. Thus, by substituting these expressions into Eq. (2) the following relation is obtained between the amplitudes of the excitation forces and the amplitudes of the harmonic responses:

$$\boldsymbol{Q}(\omega,\Omega)=\boldsymbol{H}(\omega,\Omega)\boldsymbol{F}(\omega) \tag{3}$$

where the receptance or frequency response function (FRF) matrix is expressed as follows:

$$\boldsymbol{H}(\omega,\Omega)=\left[\boldsymbol{K}+i\omega(\boldsymbol{C}+\Omega\boldsymbol{G})-\omega^2\boldsymbol{M}\right]^{-1} \tag{4}$$

## Parameterization of the Deterministic FE Model

At this point, it is important to consider that, in order to study the system behavior when uncertainties are to be considered, the random responses have to be computed with respect to a set of uncertain geometrical and/or physical parameters associated with the flexible rotor. In general, such random variables intervene in a rather complicated manner in the finite element matrices. Hence, for evaluating the variability of the responses associated with these uncertainties, it becomes interesting to perform a *parameterization* of the FE model, which is understood as a means of making the design parameters factored-out of the elementary matrices. At the expense of lengthy algebraic manipulations, this procedure makes it possible to introduce not only the uncertainties into the flexible rotor model, but also to perform a sensitivity analysis in a straightforward way, leading to significant cost savings in iterative robust optimization and/or model updating processes. After manipulations, those parameters of interest can be factored-out of the elementary matrices as indicated below:

$$shaft:\begin{cases}\boldsymbol{M}_S^{(e)}=\rho_S A_S\overline{\boldsymbol{M}}_S^{(e)}\\ \boldsymbol{K}_S^{(e)}=E_S I_S\overline{\boldsymbol{K}}_S^{(e)}\\ \boldsymbol{G}_S^{(e)}=\rho_S I_S\overline{\boldsymbol{G}}_S^{(e)}\end{cases} \tag{5.a}$$

$$bearings:\begin{cases}\boldsymbol{K}_B^{(e)}=k_{xx}\overline{\boldsymbol{K}}_{B_1}^{(e)}+k_{zz}\overline{\boldsymbol{K}}_{B_3}^{(e)}\\ \boldsymbol{C}_B^{(e)}=d_{xx}\overline{\boldsymbol{C}}_{B_1}^{(e)}+d_{zz}\overline{\boldsymbol{C}}_{B_3}^{(e)}\end{cases} \tag{5.b}$$

where $\rho_S$, $A_S$, $I_S$ and $E_S$ represent, respectively, the mass density, the cross-section area, the inertia and the Young's modulus of the shaft. $d_{xx}$, $d_{zz}$ and $k_{xx}$, $k_{zz}$ designate, respectively, the damping and stiffness coefficients of the bearings.

It is worth mentioning that the matrices appearing in the right hand side of Eqs. (5) are those from which the design parameters of interest have been factored-out.

## Stochastic Modeling of a Flexible Rotor

In order to model the system behavior when uncertainties are present in the shaft and bearing elements, the design parameters which have been factored-out of the elementary matrices appearing in expressions (5) are considered to be random. In this paper, the well-known Karhunen-Loève (KL) decomposition, which is a continuous representation for random fields expressed as the superposition of orthogonal random variables weighted by deterministic spatial functions (Ghanem and Spanos, 1991), is used. According to this technique, a random field can be viewed as a spatial extension of a random variable that describes the spatial correlation of a structural parameter that fluctuates randomly (de Lima et al., 2010). A one-dimensional random field $H(y,\theta)$ can be defined by its mean value, $E(y)=\varepsilon[H(y,\theta)]$, and its covariance function $C(y_1,y_2)=\varepsilon\{[H(y_1,\theta)-E(y_1)][H(y_2,\theta)-E(y_2)]\}$, where $y$ denotes the spatial dependence of the field, $\theta$ represents a random process, and $\varepsilon(\bullet)$ is the expectation operator (Nieuwenhof and Coyette, 2003).

For a one-dimensional homogeneous Gaussian random field, it is possible to find a single projection of $H(y,\theta)$ on an orthonormal truncated random basis as follows (Ghanem and Spanos, 1991):

$$H(y,\theta)=E(y)+\sum_{r=1}^{n}\sqrt{\lambda_r}\,f_r(y)\xi_r(\theta) \tag{6}$$

where the deterministic functions $f_r(y)$ and the scalar values $\lambda_r$ are, respectively, the eigenfunctions and the eigenvalues of the covariance $C(y_1,y_2)$. Also, the eigenfunctions $f_r(y)$ and the random variables $\xi_r(\theta)$ are orthonormal.

The KL expansion is defined with respect to a particular geometric domain $\Omega_{KL}$, so that in the case of modeling an uncertain parameter of a structural model by means of a random field, this geometry includes at least the domain of the structure under consideration. Furthermore, for relatively simple geometric configurations, such as the one-dimensional flexible rotor model shown in Fig. 1, the analytical solution of the eigenproblem proposed by Ghanem and Spanos (1991) for the KL expansion into the domain, $\Omega_y=(y_1,y_2)$, is given by:

$$C(y_1,y_2)=\exp\left(-|y_1-y_2|/L_{cor,y}\right) \tag{7}$$

where $(y_1,y_2)\in[0,L]$ and $L_{cor,y}$ indicates the correlation length characterizing the decreasing behavior of the covariance with the distance between the observation points in the $y$ direction. Also, it can be noted that this continuous model of covariance function corresponds to homogeneous Gaussian stochastic fields.

Taking into account the property of the covariance function, the eigenvalues and eigenfunctions are given as a function of the roots $\omega_r(r\geq 1)$ of two transcendental equations in a procedure summarized as follows:

- For $r$ odd, with $r\geq 1$:

$$\lambda_r=\frac{2L_{cor,y}}{L_{cor,y}^2\omega_r^2+1},\quad f_r(y)=\alpha_r\cos(\omega_r y) \tag{8.a}$$

where $\alpha_r=1\Big/\sqrt{L/2+\sin(\omega_r L)/2\omega_r}$ and the root $\omega_r$ is the solution of the following transcendental equation:

$$1+L_{cor,y}\,\omega_r\tan(\omega_r L)=0 \tag{8.b}$$

defined into the domain $\left[(r-1)\frac{\pi}{L},\left(r-\frac{1}{2}\right)\frac{\pi}{L}\right]$.

- For $r$ even, with $r \geq 1$:

$$\lambda_r = \frac{2L_{cor,y}}{L_{cor,y}^2 \omega_r^2 + 1}, \quad f_r(y) = \alpha_r \sin(\omega_r y) \tag{9.a}$$

where $\alpha_r = 1/\sqrt{L/2 - \sin(\omega_r L)/2\omega_r}$ and the root $\omega_r$ is the solution of the following transcendental equation:

$$L_{cor,y}\, \omega_r + \tan(\omega_r L) = 0 \tag{9.b}$$

defined into the domain $\left[\left(r - \frac{1}{2}\right)\frac{\pi}{L}, r\frac{\pi}{L}\right]$.

For illustration purposes Figs. 2 and 3 represent the graphs of the first four eigenfunctions of the covariance function (7) for two cases, respectively: first, by assuming $L_{cor,y} = 1m$ and $\Omega_y = [0, 1]$; and second, by considering $L_{cor,y} = 10m$ and $\Omega_y = [0, 10]$. The first four eigenvalues of the covariance function are the following: for the first test case $\lambda_1 = 0.7388$, $\lambda_2 = 0.1380$, $\lambda_3 = 0.0451$, $\lambda_4 = 0.0213$; for the second case $\lambda_1 = 7.3881$, $\lambda_2 = 1.3800$, $\lambda_3 = 0.4509$, $\lambda_4 = 0.2133$.

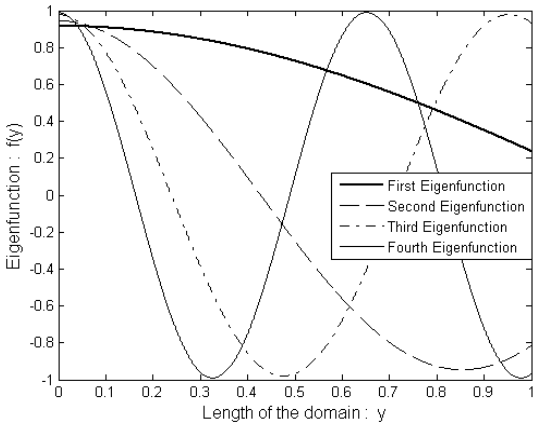


**Figure 2. Graphs of the first four eigenfunctions of the covariance for $L_{cor,y} = 1m$ and $\Omega_y = [0, 1]$.**

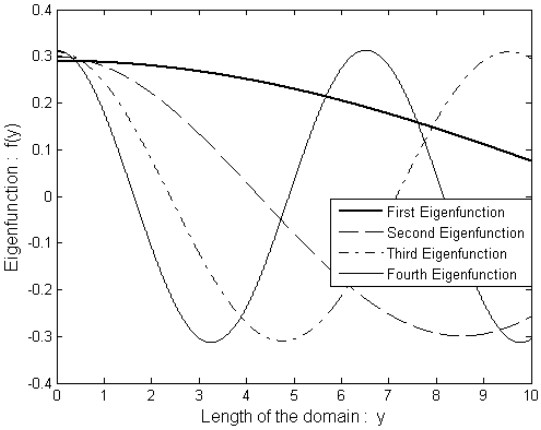


**Figure 3. Graphs of the first four eigenfunctions of the covariance for $L_{cor,y} = 10m$ and $\Omega_y = [0, 10]$.**

It can be noted that both the correlation length of the random field and the length of the definition domain influence the eigenvalues and eigenfunctions.

The expansion detailed previously has been chosen in order to model the elementary random matrices of the shaft element, as follows:

$$\boldsymbol{M}_S^{(e)}(\theta) = \boldsymbol{M}_S^{(e)} + \sum_{r=1}^{n} \overline{\boldsymbol{M}}_{S_r}^{(e)} \xi_r(\theta) \tag{10.a}$$

$$\boldsymbol{K}_S^{(e)}(\theta) = \boldsymbol{K}_S^{(e)} + \sum_{r=1}^{n} \overline{\boldsymbol{K}}_{S_r}^{(e)} \xi_r(\theta) \tag{10.b}$$

$$\boldsymbol{G}_S^{(e)}(\theta) = \boldsymbol{G}_S^{(e)} + \sum_{r=1}^{n} \overline{\boldsymbol{G}}_{D_r}^{(e)} \xi_r(\theta) \tag{10.c}$$

where $\boldsymbol{M}_S^{(e)}$, $\boldsymbol{K}_S^{(e)}$ and $\boldsymbol{G}_S^{(e)}$ are the mean elementary matrices computed according to Eqs. (1) and the random matrices are computed as follows:

$$\overline{\boldsymbol{M}}_S^{(e)}(\theta) = \int_{y=0}^{L} \sqrt{\lambda_r}\, f_r(y) \boldsymbol{N}_{mi}^T(y) \boldsymbol{N}_{mi}(y) dy \tag{11.a}$$

$$\overline{\boldsymbol{G}}_S^{(e)}(\theta) = \int_{y=0}^{L} \sqrt{\lambda_r}\, f_r(y) \boldsymbol{N}_g^T(y) \boldsymbol{N}_g(y) dy \tag{11.b}$$

$$\overline{\boldsymbol{K}}_S^{(e)}(\theta) = \int_{y=0}^{L} \sqrt{\lambda_r}\, f_r(y) \boldsymbol{B}^T(y) \overline{\boldsymbol{E}} \boldsymbol{B}(y) dy \tag{11.c}$$

where $\overline{\boldsymbol{E}}$ represents the elastic material property matrix in which the parameters $E_S$, $A_S$ and $I_S$ have been factored-out.

It must be emphasized that in the simulations that follow, the choice of the uncertain parameters associated with the shaft and the bearings according to the parameterization scheme (5) are considered as being the relevant random variables to be taken into account. It should be pointed out that the bearing parameters have to be identified since they are not available in real applications. Also, as the damping and stiffness coefficients of the applied discrete bearings have been factored-out from the elementary matrices of such elements obtained by applying a dyadic structural transformation rather than an integration scheme as it is the case for the shaft, the corresponding uncertainties are introduced in a different way, by using the relations $k(\theta) = k_0 + k_0 \delta_k \xi(\theta)$ and $d(\theta) = d_0 + d_0 \delta_d \xi(\theta)$, where $k_0$ and $d_0$ designate, respectively, the mean values of the stiffness and damping coefficients of the bearings with the corresponding dispersion levels $\delta_k$ and $\delta_d$, respectively, where $\xi(\theta)$ represents a Gaussian random variable.

Having obtained the stochastic finite element matrices and after performing the standard FE matrix assembling procedure, the frequency domain random equations of motion for the stochastic flexible rotor subjected to a deterministic harmonic excitation can be expressed as follows:

$$\boldsymbol{Q}(\omega, \Omega, \theta) = \left\{\boldsymbol{K}(\theta) + i\omega[\boldsymbol{C}(\theta) + \Omega \boldsymbol{G}(\theta)] - \omega^2 \boldsymbol{M}(\theta)\right\}^{-1} \boldsymbol{F}(\omega) \tag{12}$$

where $\boldsymbol{M}(\theta)$, $\boldsymbol{C}(\theta)$, $\boldsymbol{G}(\theta)$ and $\boldsymbol{K}(\theta)$ are the global random mass, damping, gyroscopic and elastic stiffness matrices, respectively, and $\boldsymbol{Q}(\omega,\Omega,\theta)$ designates the stochastic response.

It must be emphasize that the stochastic model of the flexible rotor system (12) is to be solved by using a stochastic solver. With this aim, and in accordance with the purpose of this paper, Monte Carlo simulation in combination with Latin-Hypercube sampling method is used (Florian, 1992). In addition, the probability distributions of the uncertainty parameters are chosen *a priori*.

## Condensation of the Stochastic Flexible Rotor Model

In most cases of industrial interest, it becomes practically impossible to compute the receptance matrix by directly inverting the dynamic stiffness matrix from Eq. (12), due to the high computation cost and storage memory required, in addition to the large number of computations of the MC samples required to evaluate the FRFs variability with granted convergence for the stochastic flexible rotor system. These difficulties motivate the use of a model condensation procedure, which aims at reducing the rotor model size and the associated computational cost, while keeping an acceptable predictive capacity of the numerical model. This can be achieved based on the assumption that the exact responses, given by the resolution of Eq. (12) for each realization $\theta$, can be approximated by projecting the response vector on a reduced vector basis as follows (Lallane and Ferraris, 1998):

$$\boldsymbol{Q}(\omega,\Omega,\theta) = \boldsymbol{T}\hat{\boldsymbol{Q}}(\omega,\Omega,\theta) \tag{13}$$

where $\boldsymbol{T} \in C^{N\times NR}$ is the transformation matrix formed column-wise by a vector basis related to the flexible rotor, $\hat{\boldsymbol{Q}}(\omega,\Omega,\theta) \in C^{NR}$ are generalized coordinates, and $NR << N$ is the number of reduced vectors in the basis. The generalized coordinates representing the contribution of each column of $\boldsymbol{T}$ are chosen arbitrarily so that the reduced model provides a reasonable predictive capacity into a given frequency bandwidth. Also, the frequency band of interest is taken into account by computing a number of normal modes of the non-gyroscopic conservative associated rotor and retaining those below a certain frequency (1.5 times the last frequency of interest is typically accepted).

By considering expressions (12) and (13), the receptance matrix of the stochastic model can be rewritten as follows:

$$\hat{\boldsymbol{H}}(\omega,\Omega,\theta) = \left\{ \hat{\boldsymbol{K}}(\theta) + i\omega\left[\hat{\boldsymbol{C}}(\theta) + \Omega\hat{\boldsymbol{G}}(\theta)\right] - \omega^2 \hat{\boldsymbol{M}}(\theta) \right\}^{-1} \tag{14}$$

where $\hat{\boldsymbol{K}} = \boldsymbol{T}^T\boldsymbol{K}(\theta)\boldsymbol{T}$, $\hat{\boldsymbol{C}}(\theta) = \boldsymbol{T}^T\boldsymbol{C}(\theta)\boldsymbol{T}$, $\hat{\boldsymbol{G}}(\theta) = \boldsymbol{T}^T\boldsymbol{G}(\theta)\boldsymbol{T}$ and $\boldsymbol{M}(\theta) = \boldsymbol{T}^T\boldsymbol{M}(\theta)\boldsymbol{T}$ are the reduced matrices.

For models containing viscous or structural damping, it is relatively common to use constant projection basis formed by the eigenvectors of the associated conservative structure, as the matrices are invariant. However, for rotor systems, the selection of the reduction basis is more delicate as this condition does not hold. Due to the dependence of the gyroscopic matrix with respect to rotation speeds of the shaft, the reduction basis should be able to represent the changes of the dynamic behavior of the rotor as rotation speed is varied in a band of interest. In this work, the strategy proposed consists in using a reduction basis formed by a constant modal basis of the deterministic non-gyroscopic conservative associated system ($\Omega = 0$). Thus, the basis can be obtained by the resolution of the following eigenvalue problem:

$$\begin{gathered} \left(\boldsymbol{K} - \lambda_i \boldsymbol{M}\right)\boldsymbol{\varphi}_i = 0 \qquad i = 1,\ldots,N \\ \boldsymbol{\varphi}_0 = \left[\boldsymbol{\varphi}_1 \quad \boldsymbol{\varphi}_2 \quad \ldots \quad \boldsymbol{\varphi}_{NR}\right], \quad \boldsymbol{\Lambda}_0 = diag\left(\lambda_1,\ldots,\lambda_{NR}\right) \end{gathered} \tag{15}$$

Thus, the nominal basis of reduction for the non-gyroscopic conservative associated rotor system is given as follows:

$$\boldsymbol{T} = \boldsymbol{\varphi}_0 \tag{16}$$

## Numerical Applications

In this section, numerical simulations are presented in order to illustrate the main features and capabilities of the stochastic rotor finite element modeling methodology. In the simulations that follow the flexible rotor shown in Fig. 4 is considered as composed by a horizontal flexible steel shaft discretized into 20 Euler-Bernoulli's beam elements, two rigid steel discs ($D_1$ and $D_2$) and three asymmetric bearings($B_1$, $B_2$ and $B_3$). The values of the physical and geometrical characteristics used to generate the FE model are given in Tab. 1.

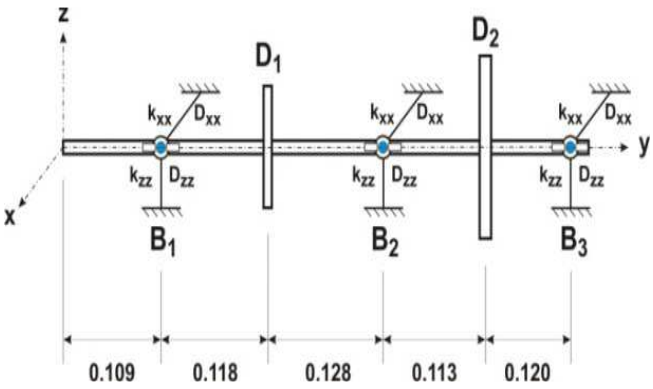


**Figure 4. Scheme of the flexible rotor system used in the simulations.**

**Table 1. Physical and geometrical properties of the rotor system.**

| Elements | Properties | Values |
|---|---|---|
| Shaft | Length (m) | 0.588 |
| | Diameter (m) | 0.010 |
| | Young's Modulus (Pa) | $2.0 \times 10^{11}$ |
| | Density (Kg/m$^3$) | 7800 |
| $D_1$ | Thickness (m) | 0.005 |
| | Diameter (m) | 0.100 |
| | Density (Kg/m$^3$) | 7800 |
| $D_2$ | Thickness (m) | 0.010 |
| | Diameter (m) | 0.150 |
| | Density (Kg/m$^3$) | 7800 |
| $B_1$, $B_2$, $B_3$ | $k_{xx}$ (N/m) | $49 \times 10^3$ |
| | $k_{zz}$ (N/m) | $60 \times 10^3$ |
| | $D_{xx}$ (Ns/m) | 5.0 |
| | $D_{zz}$ (Ns/m) | 7.0 |
| Proportional coefficients | $\alpha$ | $1.0 \times 10^{-1}$ |
| | $\beta$ | $1.0 \times 10^{-5}$ |

In a first step, one is interested in verifying the accuracy of the reduced deterministic model of the flexible rotor. The computations consist in obtaining the reduced dynamic response FRF $\hat{\boldsymbol{H}}(\omega,\Omega)$ in the frequency band [0-250 Hz], comprising the first four vibration modes of the flexible rotor, corresponding to the displacement at point $B_2$ in direction $x$ for an excitation applied in the same direction at point $D_1$, which have been chosen arbitrarily. One considers two nominal bases of reduction: (a) $\boldsymbol{T}_1 = \boldsymbol{\varphi}_0(3)$ (3 eigenvectors, computed according to Eq. (16)); (b) $\boldsymbol{T}_2 = \boldsymbol{\varphi}_0(6)$ (6 eigenvectors). These bases have been computed from the model corresponding to the nominal values of the design parameters defined in Table 1.

Figures 5 and 6 represent the amplitudes of the FRFs computed by using the two bases of reduction, as compared to the amplitudes of the FRF computed by using a reference basis formed by a far larger number of eigenvectors (30). It can be clearly seen that the use of the second basis represents quite accurately the dynamic behavior of the flexible rotor system into the frequency band of interest.

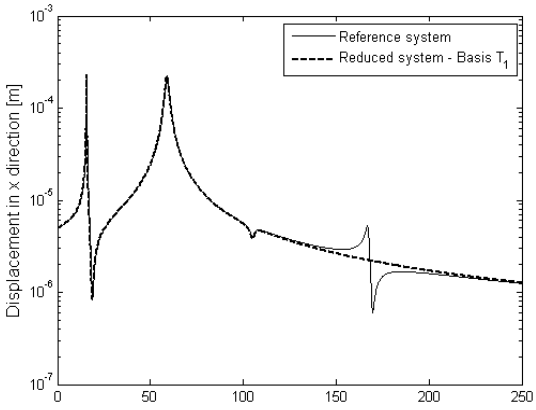


**Figure 5. FRF amplitudes of the reference and reduced systems by using the basis $\boldsymbol{T}_1$.**

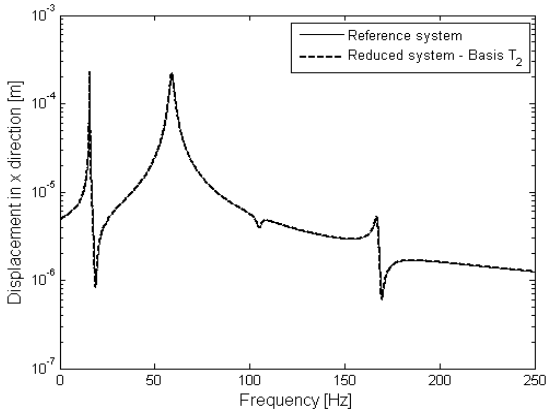


**Figure 6. FRF amplitudes of the reference and reduced systems by using the basis $\boldsymbol{T}_2$.**

In the sequence, the interest is to verify the convergence of the response variability of the stochastic model regarding the number of terms retained in the truncated KL expansion series ( $n_{KL}$ ) and the number of samples ( $n_s$ ) used in the Monte Carlo simulation. For the numerical simulations, a mean-square convergence analysis (RMS) with respect to independent realizations $\theta$ of the reduced dynamic response of the stochastic rotor model, $\hat{\boldsymbol{H}}(\omega,\Omega,\theta)$, was performed according to the following expression:

$$RMS = \sqrt{\frac{1}{n_s}\sum_{j=1}^{n_s}\left|\hat{\boldsymbol{H}}_j(\omega,\Omega,\theta) - \hat{\boldsymbol{H}}_j(\omega,\Omega)\right|^2} \qquad (17)$$

where $\hat{\boldsymbol{H}}(\omega,\Omega)$ represents the reduced response calculated for the corresponding deterministic model of the flexible rotor.

Equation (17) has been performed *a priori* for the two test scenarios depicted in Table 2 (identified as (*a*) and (*b*)) for the different dispersion levels of the random parameters related to the shaft, in order to determine the values of $n_{KL}$ and $n_s$ to be used in the numerical simulations. It must be emphasized that it has been assumed a correlation length $L_{cor,y}$ equal to the shaft finite element length according to the finite element discretization.

**Table 2. Parameters used in the convergence analysis.**

| Test scenario | $n_{KL}$ | $n_s$ |
|---|---|---|
| (*a*) | $1 \le n_{KL} \le 50$ | 100 |
| (*b*) | 10 | $1 \le n_s \le 250$ |

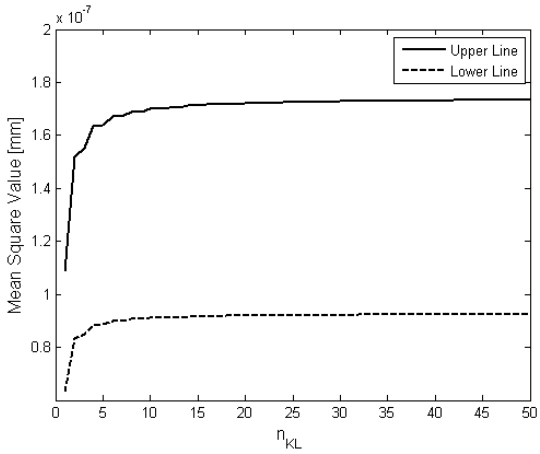


**Figure 7. Convergence in the mean-square sense for the number of terms retained in the KL expansion.**

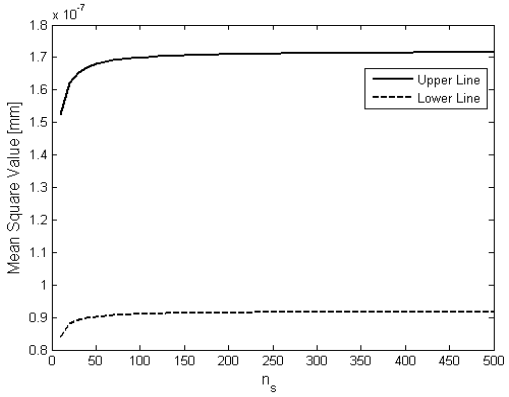


**Figure 8. Convergence in the mean-square sense for the number of samples used in the MC simulation.**

Figures 7 and 8 present, respectively, the convergence results in the mean-square sense for $n_{KL}$ and $n_s$. It is worth mentioning that the computations consist in obtaining the RMS values for both upper and lower limits of the envelopes of the amplitudes of the random FRF $\hat{\boldsymbol{H}}(\omega,\Omega,\theta)$. It has been verified that the solutions always converge for $n_{KL} \geq 10$ and $n_s \geq 70$.

To provide a sense of the degree of influence of the uncertainties introduced in the random variables over the amplitudes of the FRFs, the Campbell's diagrams and the orbits of the flexible rotor system were computed for the four test scenarios depicted in Table 3 (identified as (*a*), (*b*), (*c*) and (*d*)). The computations of the stochastic matrices of the shaft element are performed by assuming the correlation length $L_{cor,y} = 0.02725\,m$, corresponding to the length of the beam elements, according to FE mesh.

**Table 3. Definition of the uncertainty scenarios used in the simulations.**

| Scenarios | Shaft | Bearings | | | |
|---|---|---|---|---|---|
| | $E_S$ | $k_{xx}$ | $k_{zz}$ | $d_{xx}$ | $d_{zz}$ |
| (*a*) | 5% | — | — | — | — |
| (*b*) | 10% | — | — | — | — |
| (*c*) | — | 5% | 5% | 5% | 5% |
| (*d*) | 5% | 5% | 5% | 5% | 5% |

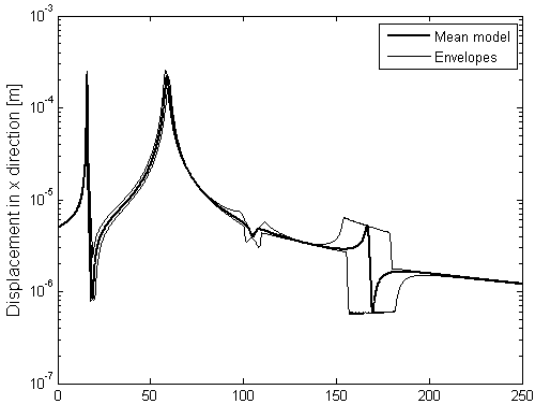


**Figure 9. Envelopes of random FRFs of the rotor for the test scenario (*a*).**

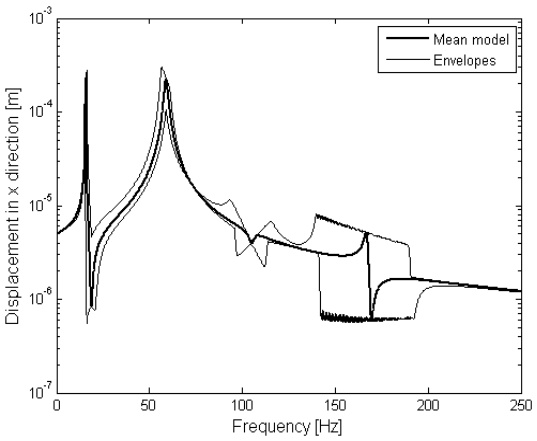


**Figure 10. Envelopes of random FRFs of the rotor for the test scenario (*b*).**

Figures 9 and 10 illustrate, respectively, the envelopes of the amplitudes of the random FRFs of the flexible rotor system for the dispersion levels reported by the test scenarios (*a*) and (*b*). In particular, it is possible to observe that as the parameter dispersion levels increase, the response dispersions increase accordingly, being larger for higher frequencies. Thus, as the frequency increases, the confidence region (the confidence that the dynamic response will be inside the envelope) becomes larger, showing the larger influence of uncertainties at high frequencies. Also, it must be emphasized that the limits of the samples enclose the amplitudes of the frequency response functions of the mean model of the flexible rotor.

In order to investigate the degree of influence of the variability on the Young's modulus of the shaft over the critical speeds of the flexible rotor, the Campbell diagram corresponding to the test scenario (*a*) has been computed, as illustrated in Fig. 11. As expected, it can be clearly seen that as the critical speed increases, the confidence region becomes larger. Also, the most immediate use of such Campbell's diagram is the quantitative determination of the degree of influence of the parameter uncertainty over the critical speeds: the larger the range of the envelopes with respect to a given parameter uncertainty level, the larger the influence of this parameter on the critical speed.

As a complementary demonstration of the influence of the uncertainties on the time domain analysis of the flexible rotor system, the orbits of the stochastic rotor were also computed for the uncertainty scenario (*a*), by considering a rotation speed of 600 RPM, in which the rotor operates above its first two critical speeds (supercritical rotor).

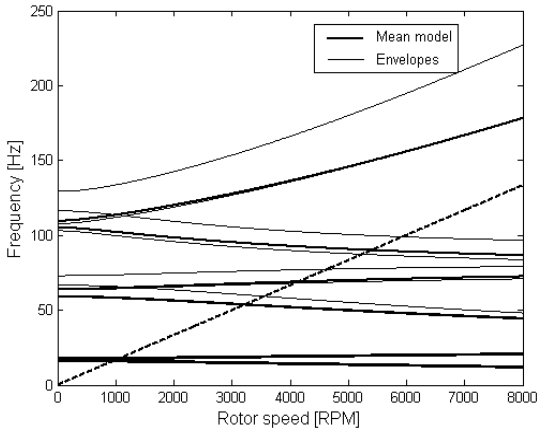


**Figure 11. Envelopes of the Campbell's diagrams for the test scenario (*a*).**

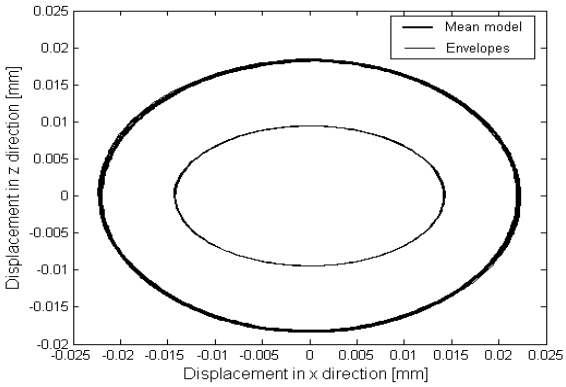


**Figure 12. Envelopes of the orbits for the test scenario (*a*).**

As can be seen in Fig. 12, the influence of the uncertainties in the amplitude of the displacement is not negligible. In addition, it is possible to conclude that this influence is more evident in the inner orbit, since the outer orbit is close to the response of the mean model of the flexible rotor.

Figure 13 shows the amplitudes of the random FRFs for the test scenario (*c*) reported in Table 3. By comparing Figs. 13 and 9 it can be noted that contrary to what has been observed in the previous example (for test scenario (*a*) or (*b*)), in which the elastic modulus of the shaft has been taken as uncertain, the dispersion of the random amplitudes of the frequency response functions do not becomes larger as the frequency increases. This is confirmed by noting a small confidence region around the critical speed of 165 Hz for the test scenario (*c*) when compared to the confidence region corresponding to the same critical speed for the test scenario (*a*) or (*b*). Thus, the trend of increased dispersions for higher frequencies is not noticed. This can be explained by observing the nominal values of the stiffness parameters of the bearings as compared to the stiffness of the shaft itself.

In terms of the Campbell diagram, Fig. 14 shows that the variations of the critical speeds associated with the test scenario (*c*) are smaller than that observed for the test scenario (*a*) (see Fig. 11). This point enables to conclude that the uncertainty introduced in the elastic material modulus of the shaft has more influence on the response of the flexible rotor system than that introduced in the parameters associated with the bearings.

Figure 15 depicts the random response of the rotor system in terms of the orbits. Also, by comparing Figs. 15 and 12, it can be perceived that the uncertainties introduced on the parameters of the bearings result in a significant change in the localized stiffness of the flexible rotor, resulting in a small variation in its displacement as illustrated in Fig. 15. This behavior is related to the values used for the stiffness parameters of the bearings as compared with the stiffness of the shaft.

It must be also noted that for all the test scenarios investigated, the limits of the samples enclose the dynamic responses of the mean model of the flexible rotor. Clearly, it should be reminded that this kind of reasoning is strictly dependent on the uncertainties levels introduced on the random variables.

Figures 16 to 18 show the envelopes of the random responses of the flexible rotor system for the test scenario (*d*). The most immediate consequence is the great influence of the introduced uncertainties on the dynamic responses of the flexible rotor. In particular, by examining the amplitudes of the random FRFs, the influence of the uncertainty on the Young's modulus is observed in the highest critical speed, while the uncertainties in the bearings cause more influence on the first two critical speeds. This aspect is also shown in the Campbell diagram illustrated in Fig. 17. Nevertheless, in terms of the orbits, the uncertainties in the parameters of the bearings influence the outer orbit and the uncertainty introduced in the shaft influences the inner orbit, as demonstrated by Fig. 18.

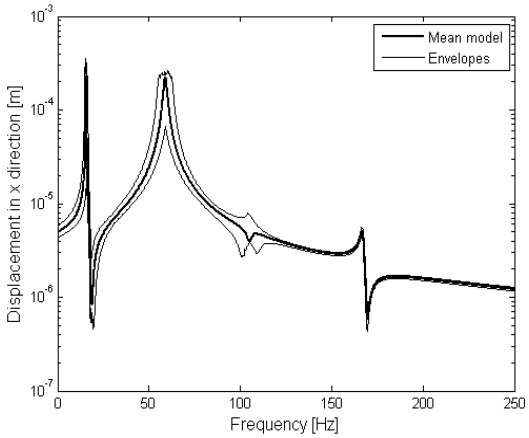


**Figure 13. Envelopes of random FRFs of the rotor for the test scenario (*c*).**

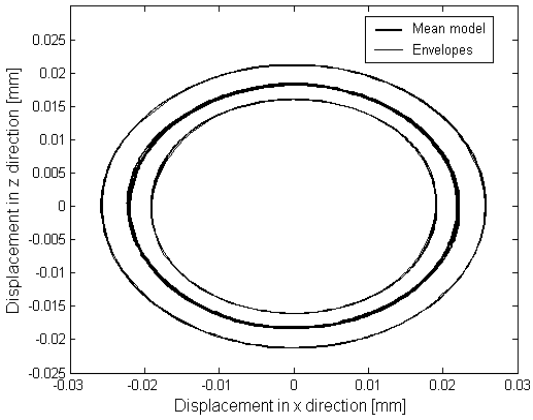


**Figure 15. Envelopes of the orbits for the test scenario (*c*).**

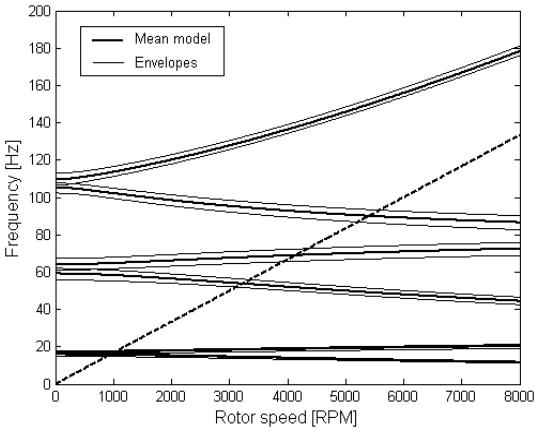


**Figure 14. Envelopes of the Campbell's diagrams for the test scenario (*c*).**

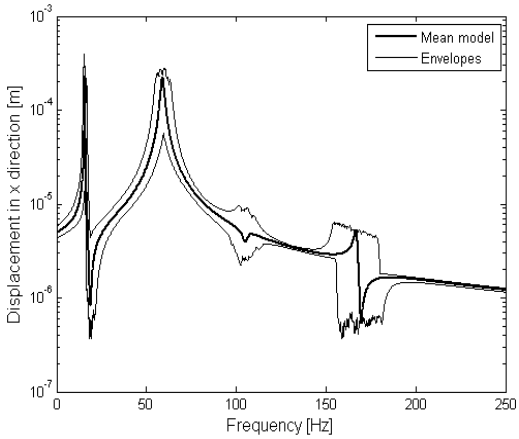


**Figure 16. Envelopes of random FRFs of the rotor for the test scenario (*d*).**

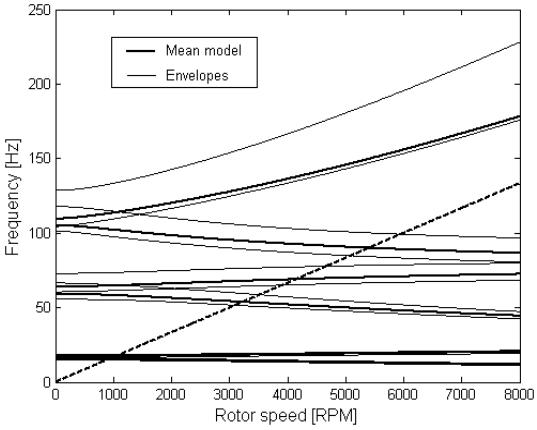


**Figure 17. Envelopes of the Campbell's diagrams for the test scenario (*d*).**

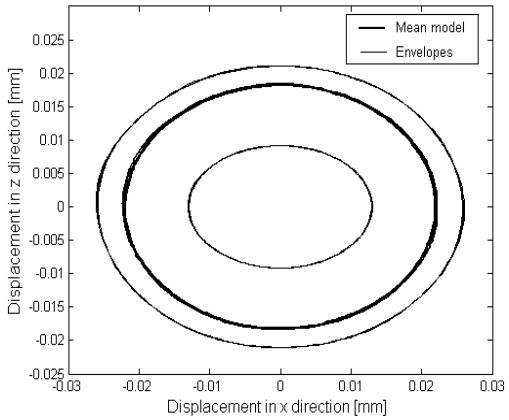


**Figure 18. Envelopes of the orbits for the test scenario (*d*).**

The general trend observed is that the dispersion of the responses increase as the number of random variables is increased, as expected. Also, for all the test scenarios investigated, the limits of the samples enclose the dynamic responses of the mean model of the flexible rotor.

## Concluding Remarks

In this paper the stochastic modeling of a flexible rotor system was proposed and implemented. The uncertainties in the design variables that characterize the flexible rotor system are introduced directly through a parametric approach, by performing a Monte Carlo simulation based on the Latin Hypercube sampling approach.

The numerical applications show that the envelopes of the random responses convey valuable information regarding the degree of influence of the random variables on the dynamic behavior of the flexible rotor. Thus, the presented procedure has proved to be a useful tool for the design and analysis of modified rotor systems and structural optimization.

The choice of the design variables (modulus of elasticity of the shaft and the parameters of the bearings) as uncertain parameters was made based on previous knowledge regarding their sensitivities with respect to the frequency response functions. It is worth mentioning that these parameters are directly associated with the dynamic behavior of the rotor as represented by the rotor orbits for the various test scenarios investigated. Thus, as demonstrated by the numerical results, the uncertainties introduced in the parameters associated with the shaft and bearings represent an important aspect to be investigated during the design phases of a flexible rotor system, due to their great influence on the critical speeds.

It must be emphasized that the limitations of the adopted discretization procedure of the random variables regarding the previous knowledge of the probability distribution function of the stochastic variables should not be disregarded.

Finally, the proposed strategy demonstrates the relevance of introducing uncertainties in the design variables from the general design perspective of rotating machinery. Further studies will encompass non-parametric studies and new applications of uncertainties analyses in rotor active control and the balancing of complex flexible rotors. Also, localized nonlinearities will be included in the rotor system.

## Acknowledgements

The third author is grateful for the support provided by the Brazilian Research Council–CNPq through the research project 308310/2010-1. The authors express their acknowledgements to the National Institute of Science and Technology of Smart Structures in Engineering (INCT-EIE), jointly funded by CNPq and FAPEMIG.

## References

Assis, E.G. and Steffen Jr., V., 2003, "Inverse Problem Techniques for the Identification of Rotor-Bearing Systems", *Inverse Problems in Engineering*, Vol. 11, pp. 39-53.

Cavalini, A.P., Galavotti, T.V., Morais, T.S., Koroishi, E.H. and Steffen Jr., V., 2011, "Vibration Attenuation in Rotating Machines Using Smart Spring Mechanism", *Mathematical Problems in Engineering* (Print), Vol. 2011, pp. 1-14.

De Lima, A.M.G., Rade, D.A. and Bouhaddi, N., 2010, "Stochastic Modeling of Surface Viscoelastic Treatments Combined with Model Condensation Procedures", *Shock and Vibration*, Vol. 17, pp. 429-444.

Florian, A., 1992, "An Efficient Sampling Scheme: Updates Latin Hypercube Sampling", *Probabilistic Engineering Mechanics*, Vol. 7**,** pp. 123-130.

Ghanem, R.G. and Spanos, P.D., 1991, "Stochastic Finite Elements - A Spectral Approach", Spring Verlag.

Guedri, M., de Lima, A.M.G., Bouhaddi, N. and Rade, D.A., 2010, "Robust Design of Viscoelastic Structures based on Stochastic Finite Element Models", *Mechanical Systems and Signal Processing*, Vol. 24, pp. 59-77.

Koroishi, E.H., Cavalini Jr, A.A., Steffen Jr., V. and Mahfoud, J., 2011, "Optimal Control of Rotor Systems Using Linear Matrix Inequalities", Proceedings of the 18th International Congress on Sound and Vibration., Rio de Janeiro.

Lallane, M. and Ferraris, G., 1998, "Rotordynamics Prediction in Engineering", John Wiley and Sons, Second Edition.

Lei, S. and Palazzolo, A., 2008, "Control of Flexible Rotor Systems with Active Magnetic Bearings", *Journal of Sound and Vibration*, Vol. 314, pp. 19-38.

Maia, N.M.M. and Montalvão e Silva, J.M., 1997, "Theoretical and experimental modal analysis", Research Studies Press LTD., England, 468 p.

Morais, T.S., Steffen Jr., V. and Mahfoud, J., 2012, "Control of the Breathing Mechanism of a cracked rotor by using electro-magnetic actuator: numerical study", *Latin American Journal of Solids and Structures* (Print), Vol. 9, pp. 581-596.

Nieuwenhof, B.V. and Coyette, J.P., 2003, "Modal Approaches for the Stochastic Finite Element Analysis of Structures with Material and Geometric Uncertainties", *Computer Methods in Applied Mechanics and Engineering*, Vol. 192, pp. 3705-3729.

Rémond, D., Faverjon, B. and Sinou, J.J., 2011, "Analysing the Dynamic Response of a Rotor System under Uncertain Parameters Polynomial Chaos Expansion", *Journal of Vibration and Control*, Vol. 18, pp. 712-732.

Ritto, T.G., Lopez, R.H., Sampaio, R. and Cursi, J.E.S.D., 2011, "Robust Optimization of a Flexible Rotor Bearing System using the Campbell Diagram", *Engineering Optimization*, Vol. 43, pp. 77-96.

Saldarriaga, M.V., Steffen Jr., V., Der Hagopian, J. and Mahfoud, J., 2010, "On the Balancing of Flexible Rotating Machines by Using an Inverse Problem Approach", *Journal of Vibration and Control*, pp. 1-13.

Sampaio, R. and Cataldo, E., 2010, "Comparing Two Strategies to Model Uncertainties in Structural Dynamics", *Shock and Vibration*, Vol. 14, pp. 171-186.

Simões, R.C., Steffen Jr, V., Der Hagopian, J. and Mahfoud, J., 2007, "Modal Active Control of a Rotor using Piezoelectric Stack Actuators", *Journal of Vibration and Control*, Vol. 13, pp. 45-64.

Vance, J., Zeidan, F. and Murphy, B., 2010, "Machinery Vibration and Rotordynamics", John Wiley & Sonsand Control, Vol. 13, pp. 45-64.